Wakes behind surface-mounted obstacles: Impact of aspect ratio, incident angle, and surface roughness

Nicolas Tobin and Leonardo P. Chamorro

Wakes behind surface-mounted obstacles:
impact of aspect ratio, incidence angle, and surface roughness

Nicolas Tobin

Department of Mechanical Science and Engineering,
University of Illinois at Urbana-Champaign, Urbana, IL 61801, USA

Leonardo P. Chamorro

Department of Mechanical Science and Engineering,
University of Illinois at Urbana-Champaign, Urbana, IL 61801, USA
Department of Civil and Environmental Engineering,
University of Illinois at Urbana-Champaign, Urbana, IL 61801, USA and
Department of Aerospace Engineering,
University of Illinois at Urbana-Champaign, Urbana, IL 61801, USA
(Dated: March 8, 2018)

The so-called wake-moment coefficient $\tilde{C}_h$ and lateral wake deflection of three-dimensional windbreaks are explored in the near and far wake. Wind-tunnel experiments were performed to study the functional dependence of $\tilde{C}_h$ with windbreak aspect ratio, incidence angle, and the ratio of the windbreak height and surface roughness (h/z_0). Supported with the data, we also propose basic models for the wake deflection of the windbreak in the near and far fields. The near wake model is based on momentum conservation considering the drag on the windbreak, whereas the far-wake counterpart is based on existing models for wakes behind surface-mounted obstacles. Results show that $\tilde{C}_h$ does not change with windbreak aspect ratios of 10 or greater; however, it may be lower for an aspect ratio of 5. $\tilde{C}_h$ is found to change roughly with the cosine of the incidence angle, and to depend strongly on h/z_0. The data broadly support the proposed wake-deflection models, though better predictions could be made with improved knowledge of the windbreak drag coefficient.

I. INTRODUCTION

The sheltering effects of windbreaks have been widely used in engineering to control erosion, and the deposition of a variety of particles including sand and snow, among others. They may be useful in the operation of wind farms; recently, Tobin *et al.* [1] showed that a local speed-up from windbreaks may be used to enhance turbine power. However, wakes from windbreaks or other obstacles far upwind may slow the wind approaching a turbine. To ensure good performance for all of the windbreak applications listed, sheltering effects must be well modeled. Several valuable contributions to windbreak-wake modeling have been made in the literature as well as in commercial softwares, such as WAsP (Wind Atlas Analysis and Application Program)[2]. Taylor and Salmon [3] provided an excellent overview of work that has taken place on two- and three-dimensional wakes, and proposed a scheme to estimate sheltering effects.

The form for the velocity deficit Δu behind a three-dimensional obstacle oriented perpendicular to the mean flow direction was suggested by Lemberg [4] as:

$$\frac{\Delta u}{U_h} = \left(\frac{x}{h}\right)^c F(\eta)G(\zeta), \tag{1}$$

where x is the streamwise distance downwind of the windbreak, U_h is the velocity of the approach flow at the windbreak height h, and η and ζ are similarity variables for the spanwise and vertical coordinates y and z. This formulation is valid only in the far wake, commonly defined as $x/h \gtrsim 10$. Values of c in the literature are generally close to -1.5, though they may be dependent on obstacle geometry, and can change slightly depending on the assumptions of the author (Taylor [5] discusses the findings of many authors who found power-law behavior). $F(\eta)$ is typically taken as a Gaussian function, whereas $G(\zeta)$ may use either the small-perturbation formulation of Counihan *et al.* [6], or the semi-empirical formulation of Perera [7]. For both forms of G, the so-called wake moment:

$$\tilde{C} = \int_0^\infty \int_{-\infty}^\infty z \Delta u U(z) dy dz, \tag{2}$$

is shown to be constant with downstream distance. The justification for equation 2 given by Counihan *et al.* [6] is rather involved, but it may be shown more simply via the conservation of angular momentum in a control volume around the windbreak, relating the quantity $\tilde{C}$ to the net overturning moment exerted on the control volume by the windbreak. Similarly, Hunt [8] shows that the same quantity is preserved in the wake of a surface-mounted obstacle in a laminar boundary layer. The quantity $\tilde{C}$ cannot be deduced simply from the forces on the obstacle, and varies based on the class of obstacle. Taylor and Salmon [3] discussed approximate values of the wake-moment coefficient $\tilde{C}_h$, defined as

$$\tilde{C}_h = \frac{\tilde{C}}{bh^2 U_h^2}, \tag{3}$$

for several classes of obstacles, where b is the obstacle width. Because of its direct derivation from the Navier-Stokes equations, we take the form of $G(\zeta)$ from Counihan *et al.* [6] to use in all subsequent analysis, using the asymptotic limit where the approach velocity profile has a power-law exponent of $n = 0$. That is, we treat the approach flow as having no shear; this has only a minimal impact on the shape of the wake profile. Combined with the Gaussian spreading of Taylor and Salmon [3] for $F(\eta)$, the resulting relation for Δu is:

$$\frac{\Delta u}{U_h} = \frac{b\tilde{C}_h Re_t}{hI} \frac{\zeta e^{-1/4\zeta^2}}{(x/h)^{3/2}} \frac{1}{\sqrt{2\pi}a_f} \exp\left(\frac{-\eta^2}{2a_f}\right). \tag{4}$$

In equation 4, $I = 7.08$ for $n = 0$, $Re_t = \ln(h/z_0)/\kappa^2$ where $\kappa = 0.4$ is the von Kármán constant, z_0 is the surface roughness of the ground and $a_f = 0.5$ as suggested by Taylor and Salmon [3]. Re_t is interpreted as a *turbulent Reynolds number*, which is the ratio of inertial forces to turbulent diffusion. The similarity variables are given as:

$$\zeta = \frac{z}{l} = \frac{z}{h\sqrt{\frac{2x}{hRe_t}}}, \tag{5}$$

where $l = h(2x/(hRe_t))^{1/2}$ is the vertical length scale defined in Counihan *et al.* [6], and

$$\eta = \frac{y/h}{\sqrt{x/h}}. \tag{6}$$

The growth of these similarity length-scales downstream accounts for entrainment into the wake. Taylor and Salmon [3] suggested simply using a value for $\tilde{C}_h$ of $0.8(1 - \phi)$, where ϕ is the obstacle porosity, for two-dimensional fences or windbreaks based on the published results of Counihan *et al.* [6] and Castro [9]. This is also the approach used in the commercial wind-energy code WAsP [10], which appears to use $\tilde{C}_h = 0.8(1 - \phi)$ for all classes of obstacles. However, this may be too severe a simplification, as $\tilde{C}_h$ should be assumed to depend on geometry and flow conditions. Taylor and Salmon [3] suggested a value of $\tilde{C}_h = 0.35$ for cubes; similarly, we will present results in the following sections that for certain flow conditions, $\tilde{C}_h$ may be as high as 1.4. This suggests that existing models could be off by a factor of 2 in either direction for some situations. Further, no accounting is made for the deflection of the wake perpendicular to the direction of flow in either the WAsP model or the model proposed by Taylor and Salmon [3]. Similar to the deflection of the wakes of wind turbines in yaw, a windbreak facing an oblique wind is expected to have a laterally deflected wake.

Among the earliest to perform measurements of the mean wind profile downwind of a porous windbreak was Nägeli [11]. Recent lidar measurements by Peña *et al.* [12] have also shown that the best fit to the formulations of Counihan *et al.* [6] may come about with different values of $\tilde{C}_h$. Windbreak wakes in oblique flow have also been extensively studied; for instance, the field measurements of Wilson [13] measured the shelter of a windbreak in oblique flow and also reported the impact of thermal stratification. Other works investigating the shelter effect behind windbreaks in oblique winds include the numerical simulations of Wang and Takle [14] and the lidar measurements of Peña *et al.* [12]. Experimental studies have further studied the impact of thermal stability, such as Seginer [15] who found a significant reduction in shelter for unstable conditions. Other works, such as that of Wang and Takle [16] who showed the impact of windbreak depth on shelter efficiency, suggest that a broader understanding of windbreak flows simply requires data to investigate various functional dependencies.

It is the goal of this work to expand the knowledge of wakes behind windbreaks by investigating the functional dependence of $\tilde{C}_h$ on the incidence angle, aspect ratio, and h/z_0, and the wake deflection on incidence angle and aspect ratio. This is explored with wind-tunnel experiments, which are outlined in Section II, and a simple theoretical formulation for lateral wake deflection described in Section III A. Relevant results are given in Section III B, and concluding remarks are made in Section IV.

II. EXPERIMENTAL SETUP

The experiments were conducted in the wind tunnel of the University of Illinois at Urbana-Champaign's Renewable Energy and Turbulent Environment Group. The Eiffel-type wind tunnel test section is 0.914 m wide, 0.457 m high and 6.10 m long and the ceiling is adjustable to control the pressure gradient. Windbreaks of optical porosity $\phi = 10\%$ were placed in a boundary layer of thickness $\delta = 0.3$ m under nearly zero pressure gradient. Wake flow was characterized for various windbreak aspect ratios AR, incidence angles θ and surface roughnesses z_0 at Reynolds number $Re = U_\infty \delta / \nu \approx 1.8 \times 10^5$. Here, U_∞ and ν indicate the freestream velocity and kinematic viscosity of the air. Hotwire anemometry was used to measure the flow at various streamwise (x), spanwise (y) and vertical (z) locations. In each location, flow was measired at a sampling frequency of 10 kHz for a period of 60 s. A schematic of the experimental setup is illustrated in figure 1. There, the origin of the coordinate system is located at the windbreak center.

Experiments focused on three distinctive sets to characterize the wake. The first series investigated the combined impact of AR and incidence angle θ on the wake moment coefficient $\tilde{C}_h$. Here, the windbreaks had $AR = b/h$ of 5, 10, 15, and 20, with height $h = 12$ mm and thickness $w = 3$ mm, for a Reynolds number $Re_h = U_\infty h/\nu = 7300$. This may indicate some Reynolds number dependence, as Reynolds-independence is generally observed for $Re_h > 10^4$ [17]. For each AR, the wake deficit was measured at $\theta = 0°$, 15°, 30°, 45°, and 60° over a nearly smooth wall with $z_0 = 0.019$ mm. The streamwise distance between the windbreak center and the hotwire was $x/h = 55$ in all cases. Velocity measurements were performed over a grid that spanned $z/h \in [1.0, 7.7]$ in the vertical, with $\Delta z/h \approx 1.7$, and $y/h \in [0, 12.5]$ in the spanwise direction with $\Delta y/h \approx 2.5$; this resulted in 66 velocity measurements for each
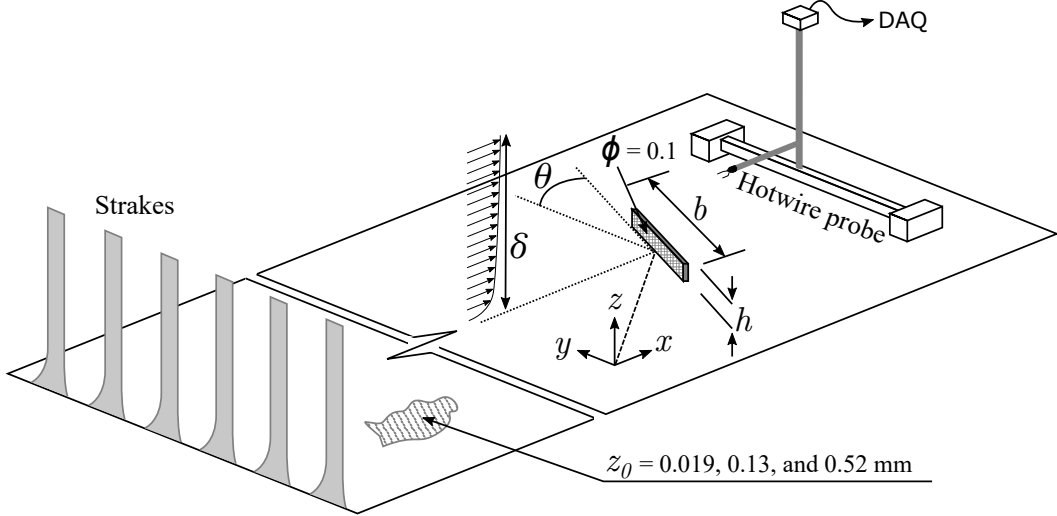
FIG. 1. Basic schematic of the experimental setup. Symbols Φ, δ and θ denote porosity, boundary layer and inclination angle. The origin of the coordinate system $(x, y, z)=(0,0,0)$ is set at the windbreak center.

combination of θ and AR. Due to constraints of the traversing system for negative y-values, measurements were made for both positive and negative incidence angles in order to quantify the asymmetric wakes.

The second series was focused on the windbreak wake deflection. This was determined with lateral velocity profiles, with the same spanwise measurement locations indicated in the first series (i.e., $y/h \in [0, 12.5]$ and $\Delta y/h \approx 2.5$), at $z/h \approx 2.7$. All the windbreaks were interrogated (all AR) at incidence angles $\theta = 15°$, $30°$, $45°$, $60°$, and $75°$ over the same wall ($z_0 = 0.019$ mm). Data were collected at streamwise locations $x/h \approx 55$ and 105 downstream of the windbreak center. In addition, lateral profiles were measured from $x/h \in [20, 50]$ every $5h$ for the single case of a windbreak with AR=10 and $\theta = 30^o$.

The last series was performed to inspect the wall roughness effects; for this purpose, the wake of several ratios of windbreak height and roughness length were characterized to determine the functional dependence of $\tilde{C}_h$ on h/z_0. Surface roughness was achieved by lining the wind-tunnel floor with B-flute single-face corrugated cardboard, with 2-mm-high flutes spaced 8 mm apart. This resulted in two different roughnesses by aligning the flutes perpendicular to ($z_0 = 0.52$ mm) and aligned with ($z_0 = 0.13$ mm) the mean flow. By using combinations of two windbreak heights ($h = 12$ mm and 24 mm, both with $b = 240$ mm) and the three roughnesses, four values of h/z_0 were investigated; $h/z_0 = 23$, 95, 190, and 635. Measurement locations included the same grid as the first series at the same downwind distance ($x/h = 55$). No non-zero incidence angles were inspected along with roughness effects, though roughness is expected to impact wake deflection, as discussed in section III A.

III. ANALYSIS

A. Models for lateral wake deflection in the near and far fields

Herein, we seek an analytical formulation of the lateral wake deflection for a windbreak at an oblique angle with respect to the mean flow. More so than for analytical formulations for the lateral deflection of wind-turbine wakes, such as that of Jiménez et $al.$ [18], the application of momentum conservation must be made with caution. When considering the wake behind an object in a freestream, the relation between the force on the object F and the velocity defect Δu,

$$F = \int_0^\infty \int_{-\infty}^\infty U(z)\Delta u(x, y, z)dydz, \tag{7}$$

where U is the local time-averaged velocity, can safely be assumed when mass conservation is accounted for. However, this is not true for the wake of surface-mounted obstacles, due to a reduction in surface shear stress induced by a reduced velocity magnitude near the ground. In fact, typical formulations for this type of wake would have the right-hand side of equation 7 approach infinity as $x \to 0$. Therefore, it is necessary to formulate a different near-wake approximation for Δu behind a surface-mounted obstacle.

Considering some location close to the windbreak, but far enough away that the pressure has returned to its atmospheric value, equation 7 may be assumed true, as the changes in surface shear do not develop enough to substantially affect the momentum balance. It should be noted that a reduction in shear is also expected upwind of the windbreak, but this is over a much shorter distance, and can be ignored (see figure 2 of Wang and Takle [14]) For a windbreak at some incidence angle θ with respect to the wind, the local force f exerted on the windbreak in the direction of θ can be estimated as

$$f = 1/2\rho C_D bh U_h^2 \cos^2(\theta), \tag{8}$$

where C_D is the windbreak's drag coefficient. If it is assumed that the force vector is perpendicular to the windbreak, the forces in the streamwise and lateral directions, f_x and f_y are then

$$f_x = 1/2\rho C_D bh U_h^2 \cos(\theta)^3 \tag{9}$$

$$f_y = 1/2\rho C_D bh U_h^2 \cos(\theta)^2 \sin(\theta) \tag{10}$$

Equations 9 and 10 are similar to equations A4 and A5 in Wilson and Flesch [19]. Note, however, that Wilson and Flesch [19] define the force projected by the barrier with a pressure coefficient k_{r0}, which acts instead on the velocity that passed through the windbreak. They also account for a local deflection angle of the approach wind by the more complicated flow in the vicinity of the windbreak, which is solved for via numerical simulation. The assumption of a local deflection further introduces the possibility of drag acting parallel to the windbreak, which is discussed in detail by Wilson [21]. In the interest of producing simple expressions for the wake deflection without numerical simulation, we proceed with the assumption that local deflection and parallel drag can be ignored, but note that this may be a source of error in our predictions. We proceed in a fashion similar to that of Jiménez et al. [18], who related the wake deflection angle α, with respect to the mean wind direction, downwind of a wind turbine to the vertical and lateral growth of an idealized top-hat profile wake. If a rectangular wake shape is assumed with width B and height H, the momentum integral projected in the x- and y-directions gives the approximate results

$$f_x \approx \rho U_h \Delta \overline{u} BH \cos(\alpha), \tag{11}$$

$$f_y \approx \rho U_h^2 BH \sin(\alpha), \tag{12}$$

where $\Delta \overline{u}$ is the average wake deficit. Then, taking equations 10 and 12 for f_y to be identical, α can be solved for with formulations for B and H. It should be assumed that at $x = 0$, $B = b \cos(\theta)$ and $H = h$. To account for the growth of B and H due to momentum entrainment past $x = 0$, we propose adding the characteristic length scale $l(x)$ from Counihan et al. [6] to h and $b \cos(\theta)$, so that

$$H = h + h\sqrt{\frac{2x}{hRe_t}} \tag{13}$$

and

$$B = b \cos(\theta) + 2h\sqrt{\frac{2x}{hRe_t}}. \tag{14}$$

Therefore, the final formulation for the near-wake deflection angle is given as

$$\sin(\alpha) = \frac{hb \cos^2(\theta) \sin(\theta) C_D/2}{\left(h + h\sqrt{\frac{2x}{hRe_t}}\right)\left(b \cos(\theta) + 2h\sqrt{\frac{2x}{hRe_t}}\right)}. \tag{15}$$
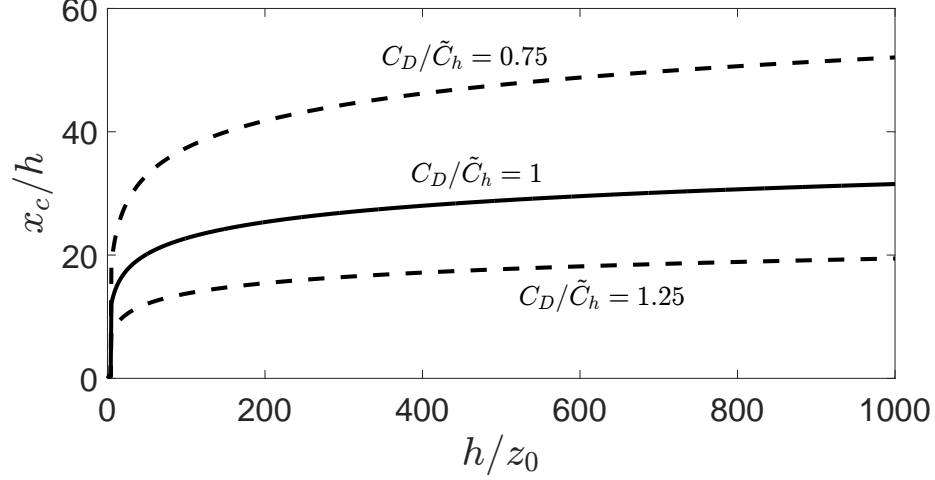
FIG. 2. Normalized cutoff location x_c/h between near and far wake of a windbreak as a function of h/z_0.

The lateral wake deflection δ_y can simply be integrated with distance, as the deflection angle is known at every downwind location. Because we have neglected the area of reduced pressure immediately in the lee of the windbreak, this analysis should apply only at intermediate distances. Further, the flow very near the windbreak may be strongly reversed and nonlinear. A wake model would therefore be inappropriate; however, equation 15 is well-behaved at $x = 0$, so we will use it as an approximation for the total effects that occur in the very near wake. This formulation is only true for distance over which the surface stress does not significantly impact the momentum valance; another deflection model should be used in the far wake. For this purpose, a cutoff distance, x_c, is defined as that location where equation 7 is true when using the wake formulation in equation 4. That is,

$$1/2\rho C_D bh U_h^2 = \int_0^\infty \int_{-\infty}^\infty U(y,z)\Delta u(x_c,y,z)dydz. \tag{16}$$

This location is dependent on h/z_0, and strongly dependent on the fraction $C_D/\tilde{C}_h$, as shown in figure 2. Therefore, lacking knowledge of C_D, an estimate must be made based on $\tilde{C}_h$. We assume that $C_D/\tilde{C}_h = \beta$, and find β with a best fit of the data. It should be noted that due to the change in the near- and far-wake models due to changes in C_D, the actual deflection predictions are only modestly affected by β as shown in figure 3. For $\beta = 1$, x_c is around double the typical values for recirculation length, as reported in figure 12 of Ogawa and Diosey [22].

Past x_c, i.e., in the far wake, we propose a formulation based on equation 4. It is assumed that the overturning moment M on the obstacle is projected with the windbreak angle, as illustrated in figure 4. Specifically, an out-of-plane component $\tilde{C}_{h,x} = \tilde{C}_h \sin(\theta)\cos(\theta)$ of the wake moment is formed from a spanwise velocity perturbation Δv, which is estimated identically to Δu according to equation 4. A characteristic value of this velocity perturbation is taken as the maximum value of Δv. This far-wake characteristic velocity deficit $\Delta\overline{v}_f$ may be solved for, from equation 4, as

$$\Delta\overline{v}_f = U_h \frac{b\tilde{C}_h Re_t \sin(\theta)\cos(\theta)}{h\sqrt{\pi e}I(x/h)^{3/2}}. \tag{17}$$

If this velocity deficit is again at the oblique angle α, it may be assumed that the wake simple advects downstream with the streamwise velocity $U_h - \Delta\overline{u}_f$ and spanwise velocity $-\Delta\overline{v}_f$. Then, if $\Delta\overline{u}_f/U_h \ll 1$,

$$\alpha \approx \frac{\Delta\overline{v}_f}{U_h} = \frac{b\tilde{C}_h Re_t \sin(\theta)\cos(\theta)}{h\sqrt{\pi e}I(x/h)^{3/2}}. \tag{18}$$

The lateral deflection is obtained by integrating the appropriate solution for α at each location. An illustrative example of the theoretical deflection is shown in figure 3 for incidence angle $\theta = 30^o$, $b/h=10$, and $\beta = 1$. It should be noted that the slope is not, in general, continuous at x_c. Additionally, the proposed wake-deflection formulations
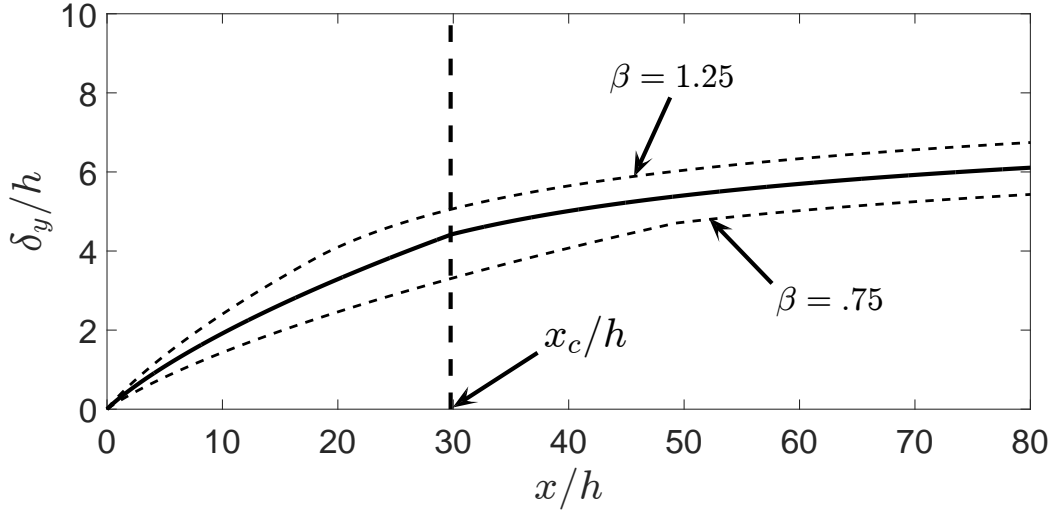
FIG. 3. Near- and far-wake estimation from the proposed models for wake deflection of a windbreak. Solid black line indicates $\beta = 1$; whereas dashed lines indicate $\beta = 1 \pm 0.25$.
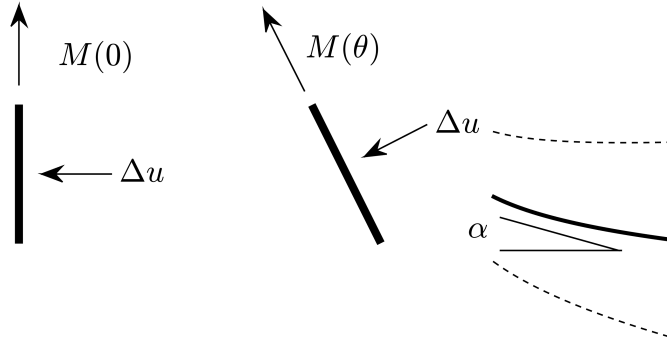

FIG. 4. A moment that is not aligned with the y-axis will lead to a perturbation velocity which is not aligned with the axis of the wind.

require knowledge of the drag coefficient C_D. We make the simplifying assumption that $C_D = \beta \tilde{C}_h$, though this should, in general, be revisited for specific geometries. According to the tabulated data in Taylor and Salmon [3], C_D is generally greater than $\tilde{C}_h$. The predictions made are moderately sensitive to C_D over realistic values; the dashed lines in figure 3 show the results of the wake deflection formulations for $\beta = 1 \pm 0.25$.

B. Evaluation of the models

Calculating $\tilde{C}_h$ from the data is challenging; this is due to the vertical coordinate z included in the integrand of equation 2. Therefore, small errors in Δu are amplified at relatively large values of z. To control the associated error, we integrated the wake moment only considering data points which equation 4 would predict to have a value for $\Delta u > 0.01 \times$ the maximum wake deficit. If equation 4 is assumed valid, the reported values of $\tilde{C}_h$ therefore have an under-reporting bias of around 2%. No accounting is made for the width of the windbreak when considering the lateral spreading of the velocity deficit. Because Taylor and Salmon [3] suggested a Gaussian spreading, an accounting for windbreak width might easily be performed by considering many differential slices of width to arrive upon an error-function type lateral profile. However, this is inconsistent with our measurements, even for the widest windbreak. All measured wake deficits had approximately Gaussian lateral spreading at $x/h = 55$, though this likely would not be the case at a location nearer to the windbreak. When evaluating equation 4 for the wakes behind windbreaks with $\theta \neq 0$, the lateral dimension is first offset with a value which is based on a least-squares fit between the data and the
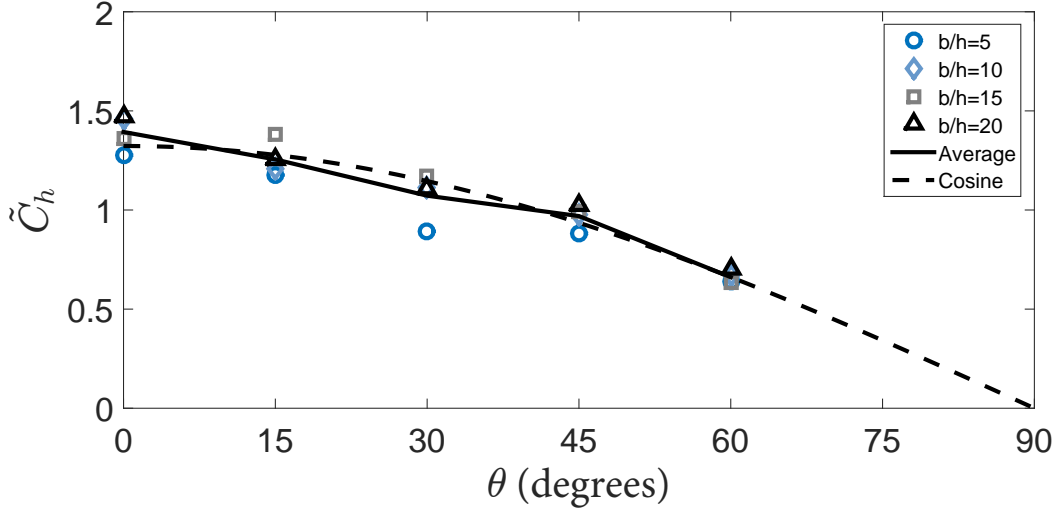
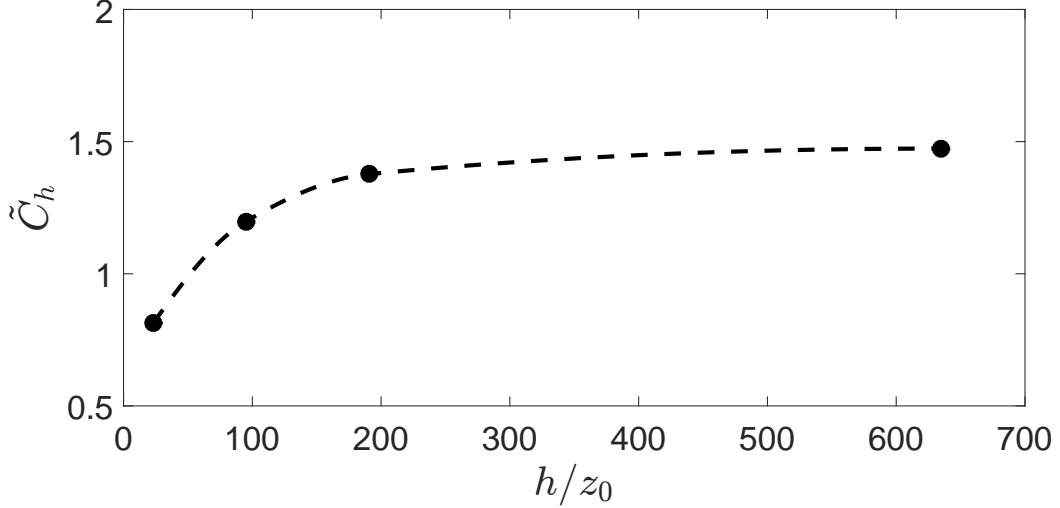FIG. 5. Wake moment coefficient $\tilde{C}_h$ for the tested $AR = b/h$ and θ.

FIG. 6. Measured wake moment coefficient $\tilde{C}_h$ as a function of h/z_0.

theoretical formulation for Δu. That is, we assume that $\Delta u \propto \exp[-0.5(y - \delta_y)^2/a^2(x)]$, where $a(x)$ is the lateral length scale, which is simultaneously varied in minimizing the squared error. This least-squares offset is reported as the wake deflection, and tested against the results of § III A.

For $h/z_0 = 634$, $\tilde{C}_h$ is found to have a 0-incidence-angle value of around 1.4 for all aspect ratios investigated, and this value decreases roughly as $\cos(\theta)$ for all aspect ratios, as shown in figure 5. This suggests that the wake strength can be assumed as being simply proportional to the projected wind-facing area. $\tilde{C}_h$ may be smaller in the case $b/h = 5$ than for the other aspect ratios, but only the values at $\theta = 30^\circ$ are statistically significant (p<0.05). Because the velocity deficits are comparatively lower for smaller AR, more uncertainty should be expected for $AR = 5$. Taylor and Salmon [3] suggested that an object with $AR = 1$ should have a $\tilde{C}_h$ around half that of one with a very large AR; if the dependence of $\tilde{C}_h$ on AR is assumed smooth, there must therefore be some critical AR where $\tilde{C}_h$ transitions between the low and high AR values. These results suggest that such a critical AR is less than 5 for this particular geometry and h/z_0.

The measured dependence of $\tilde{C}_h$ on h/z_0 is presented in figure 6. It is clear from these data that wake strength depends strongly on the underlying roughness length. This is consistent with the argument by Counihan *et al.* [6] that the wake moment has a significant contribution from the pressure perturbation in the lee of an obstacle due to
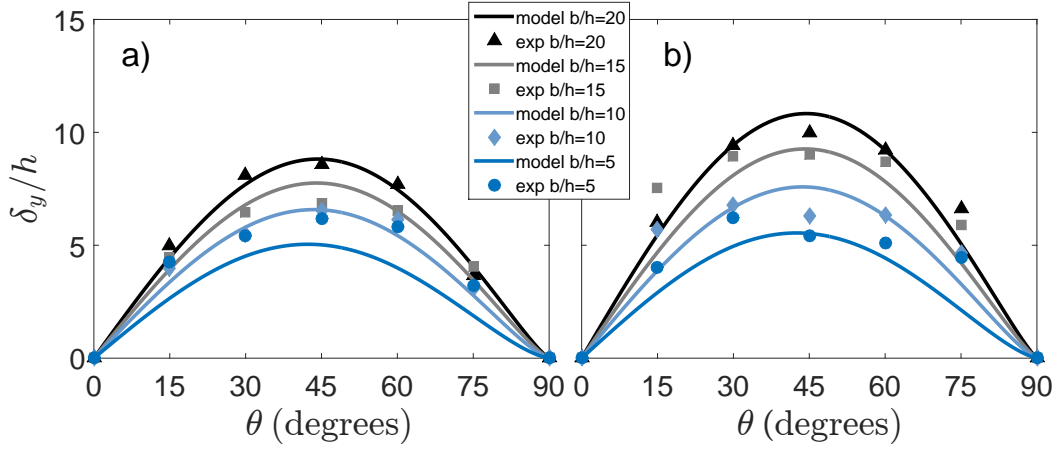
FIG. 7. Measurements (symbols) and predictions (solid lines) of the normalized wake deflection (δ/h) for all tested AR ($=b/h$) and θ. a) $x/h = 55$; b) $x/h = 105$.
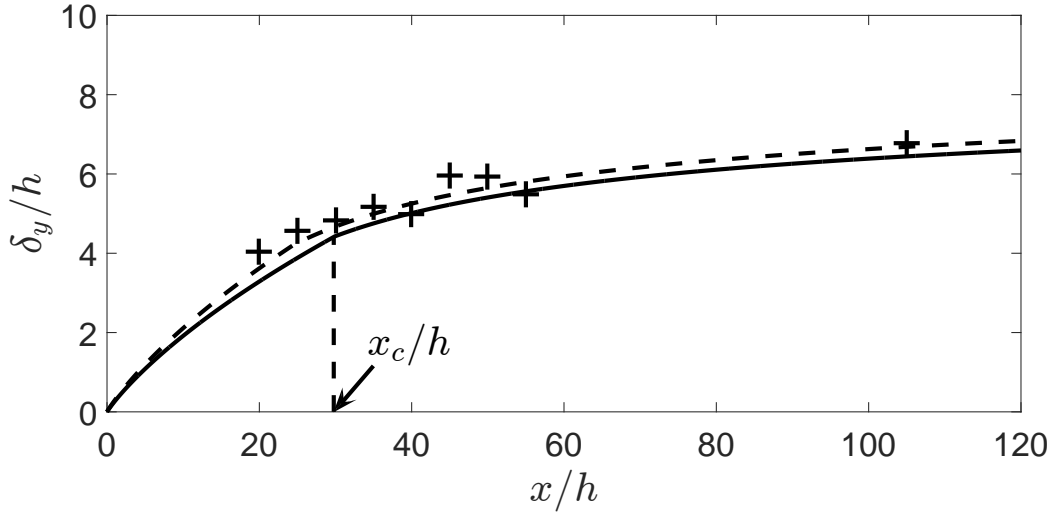

FIG. 8. Measured ($+$) and predicted (solid line for $\beta = 1$, dashed line for $\beta = 1.1$) normalized wake deflection (δ/h) at several downstream locations for a windbreak with $AR = 10$ and $\theta = 30^o$.

the presence of a recirculation zone. They argue that in the absence of a recirculation zone, the wake moment is equal to the overturning moment on the obstacle. Consequently, the wake moment coefficient should be substantially higher with a larger recirculation length L; this is defined as the distance from the windbreak where the near-ground streamwise velocity changes sign from negative to positive. It has been established that the fraction L/h is strongly dependent on h/z_0, as seen in figure 12 of Ogawa and Diosey [22]. Based on the argument that $\tilde{C}_h$ depends on L/h, this figure in Ogawa and Diosey [22] suggests that $\tilde{C}_h$ may continue to increase, even for values of h/z_0 on the order of 10^5. Measured wake deflection broadly agrees with predictions made in § III A. Unlike $\tilde{C}_h$, which did not prove to depend strongly on b/h for the values tested, the wake deflection does appear to be affected by the AR.

Data for the single case of $b/h = 10$ and $\theta = 30^o$ are presented in figure 8 at several downstream locations. As seen in this figure, the deflection is slightly underestimated near x_c. This may be attributed to the assumption that $C_D = \tilde{C}_h$; this impacts both the location x_c and the slope of the deflection in the near wake. A better fit to the data is found with a C_D value of $\sim 1.1\tilde{C}_h$, shown with a dotted line. This is consistent with the listed drag and wake moment coefficients in Taylor and Salmon [3], where C_D is generally larger than $\tilde{C}_h$.

IV. CONCLUSION

The functional dependence of windbreak wakes on aspect ratio, surface roughness and incidence angle was investigated experimentally to better inform modeling of these types of flows. Although the functional dependence of $\tilde{C}_h$ on incidence angle is apparently dependent only on front-facing area, the combined impact of incidence angle and aspect ratio shows interesting wake-deflection behavior. This observed behavior lines up well with a simple theoretical model with distinct near- and far-wake solutions for deflection.

However, it should be cautioned that more work is appropriate for higher-accuracy modeling of wakes behind general surface-mounted obstacles. The wake strength $\tilde{C}_h$ is generally accepted as being dependent on aspect ratio, though this dependence is not currently well understood. An experimental campaign to determine this functional dependence is desirable. Further, the tabulation of $\tilde{C}_h$ values for a wider range of geometries would be useful; although effort has been made toward this by Taylor and Salmon [3], some obstacles of interest may not be well represented by the existing literature.

ACKNOWLEDGMENTS

[1] N. Tobin, A. M. Hamed, and L. P. Chamorro, "Fractional flow speed-up from porous windbreaks for enhanced wind-turbine power," Bound Lay Meteorol **163(2)**, 253–271 (2017).

[2] N. G. Mortensen, D. Heathfield, L. Myllerup, L. Landberg, and O. Rathmann, *Getting started with WAsP 9*, Tech. Rep. Risø-I-2571 (EN) (Risø National Laboratory, Technical University of Denmark, Roskilde, Denmark, 2007).

[3] P. A Taylor and J. R. Salmon, "A model for the correction of surface wind data for sheltering by upwind obstacles," J Appl Meteorol **32**, 1683–1694 (1993).

[4] R. Lemberg, *On the wakes behind bluff bodies in a turbulent boundary-layer*, Ph.D. thesis, University of Western Ontario (1973).

[5] P. A. Taylor, "Turbulent wakes in the atmospheric boundary layer," in *Flow and Transport in the Natural Environment: Advances and Applications* (Springer, 1988) pp. 270–292.

[6] J. Counihan, J. C. R. Hunt, and P. S. Jackson, "Wakes behind two-dimensional surface obstacles in turbulent boundary layers," J Fluid Mech. **64**, 529–564 (1974).

[7] M. D. A. E. S. Perera, "Shelter behind two-dimensional solid and porous fences," J Wind Eng Ind Aerod **8**, 93–104 (1981).

[8] J. C. R. Hunt, "A theory for the laminar wake of a two-dimensional body in a boundary layer," J Fluid Mech **49**, 159–178 (1971).

[9] I. P. Castro, "Relaxing wakes behind surface-mounted obstacles in rough wall boundary layers," J Fluid Mech **93**, 631–659 (1979).

[10] A. Peña, A. Bechmann, D. Conti, N. Angelou, and I. Troen, *Shelter models and observations*, Tech. Rep. DTU Wind Energy-E-Report-0092 (EN) (Technical University of Denmark, Roskilde, Denmark, 2015).

[11] W. Nägeli, "Untersuchungen über die windverhltnisse im bereich von schilfrohrwänden," Mitt Schweiz Anst Forstl Versuchsw **29**, 213–266 (1953).

[12] A. Peña, A. Bechmann, D. Conti, and N. Angelou, "The fence experiment–full-scale lidar-based shelter observations," Wind Energy Sci **1**, 101–114 (2016).

[13] J. D. Wilson, "Oblique, stratified winds about a shelter fence. part i: Measurements," J Appl Meteorol **43**, 1149–1167 (2004).

[14] H. Wang and E. S. Takle, "On shelter efficiency of shelterbelts in oblique wind," Agr Forest Meteorol **81**, 95–117 (1996).

[15] I. Seginer, "Atmospheric-stability effect on windbreak shelter and drag," Bound Lay Meteorol **8**, 383–400 (1975).

[16] H. Wang and E. S. Takle, "On three-dimensionality of shelterbelt structure and its influences on shelter effects," Bound Lay Meteorol **79**, 83–105 (1996).

[17] R. Baltaxe, "Air flow patterns in the lee of model windbreaks," Arc Meteor Geophy B **15**, 287–312 (1967).

[18] Á. Jiménez, A. Crespo, and E. Migoya, "Application of a les technique to characterize the wake deflection of a wind turbine in yaw," Wind Energy **13**, 559–572 (2010).

[19] J. D. Wilson and T. K. Flesch, "Wind measurements in a square plot enclosed by a shelter fence," Bound Lay Meteorol **109(2)**, 191–224 (2003).

[20] P. J. Mulhearn, and E. F. Bradley, "Secondary flows in the lee of porous shelterbelts," Bound Lay Meteorol **12(1)**, 75–92 (1977).

[21] J. D. Wilson, "Oblique, stratified winds about a shelter fence. Part II: Comparison of measurements with numerical models," J Appl Meteorol **43(10)**, 1392–1409 (2004).

[22] Y. Ogawa and P. G. Diosey, "Surface roughness and thermal stratification effects on the flow behind a two-dimensional fenceii. a wind tunnel study and similarity considerations," Atmos Environ **14**, 1309–1320 (1980).